Supplementary Information

Excited State Deactivation in Phytochemical Flavonoids: Astragalin and Kaempferol

Michael Hymas[1†], Jacob Eller[2†], Mohammad Salehi[3†], Reza Omidyan[1,3*], Stéphane Poigny[4], Vasilios G. Stavros[1*]

[1] *School of Chemistry, University of Birmingham, Edgbaston, Birmingham B15 2TT, United Kingdom*

[2] *Department of Physics, University of Warwick, Coventry, CV4 7AL, United Kingdom*

[3] *Department of Chemistry, University of Isfahan, 73441 Isfahan, Iran*

[4] *Mibelle Group Biochemistry, Mibelle AG, Bolimattstrasse 1, CH-5033 Buchs, Switzerland*

[†] *These authors have contributed equally.*

Section 1: Experimental and Computational Details

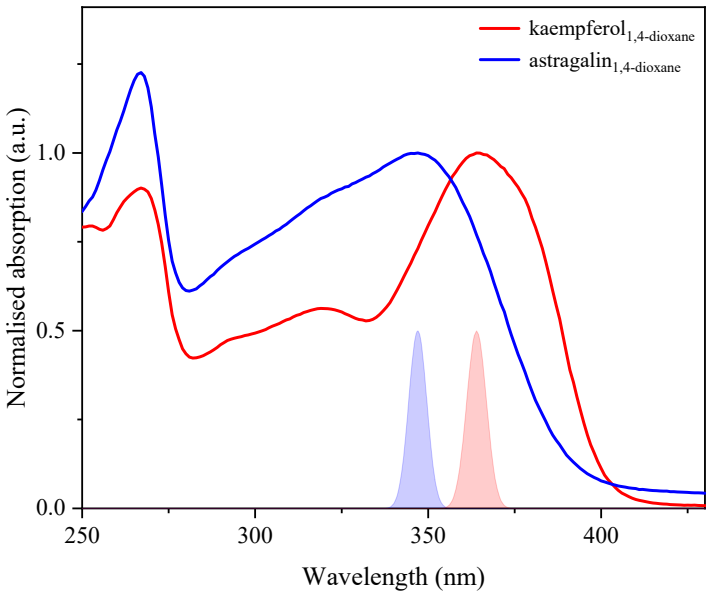

1.1. UV-visible absorption spectroscopy

Figure S1. UV-visible absorption spectra of kaempferol (red) and astragalin (blue) in 1,4-dioxane. Shaded plots are approximate profiles of the 'pump' pulses used in fs-TEAS for each solution.

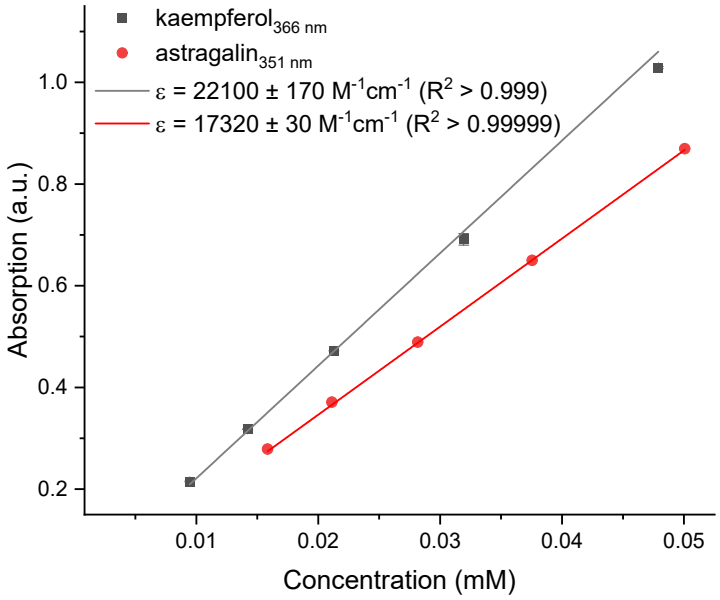

Figure S2. Plots determining extinction coefficients (slopes) for kaempferol in ethanol at 366 nm (black) and astragalin in ethanol at 351 nm (red).

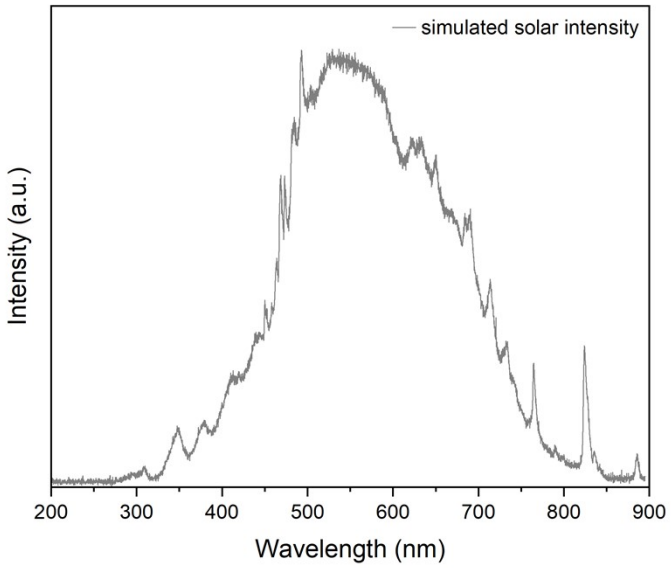

Figure S3. Simulated solar spectrum intensity.

Calculation of photostability:

Area under curve index (AUCI) is defined as the ratio of integrated absorption spectra before (A_0) and after ($A_{2\,h}$) 'solar' irradiation:

$$AUCI(\%) = 100 \times \frac{\sum_{280}^{400} A_{2\,h}(\lambda)\Delta\lambda}{\sum_{280}^{400} A_0(\lambda)\Delta\lambda}$$

$$AUCI_{kaempferol}(\%) = 100 \times \frac{28.53}{32.87} = 87\%$$

$$AUCI_{astragalin}(\%) = 100 \times \frac{20.37}{21.67} = 94\%$$

1.2. Ground state geometry determination

astragalin		
Optimized S_0	Optimized S_1	Optimized S_1/S_0 CI
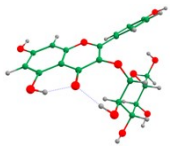	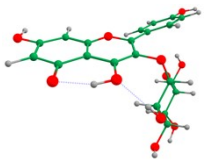	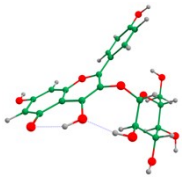
kaempferol		
Optimized S_0	Optimized S_1	Optimized S_1/S_0 CI
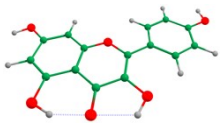	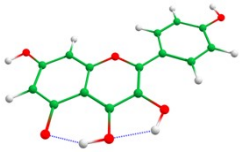	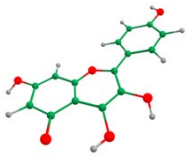

Figure S4. Optimized geometries of astragalin and kaempferol in the ground and S_1 excited state, as well as optimized S_1/S_0 conical intersection, determined at the MP2/cc-pVDZ, ADC(2)/cc-pVDZ, and CASSCF(6,6)/631G level of theory, respectively.

1.3. Vertical transition energies

Table S1. Vertical transition energies, oscillator strengths and contributing valence molecular orbitals in the S_1-S_4 electronic transitions for astragalin and kaempferol, determined at the ADC(2)/cc-pVDZ theoretical level.

Molecule	Excited state	Energy (eV)	Oscillator strength	State assignment	Molecular orbital contribution
astragalin	S_1	3.84	0.3450	$\pi\pi^*_1$	117 (HOMO) → 118 (LUMO) (64%)
				$\pi\pi^*_2$	116 (HOMO-1) → 118 (LUMO) (23%)
	S_2	4.12	0.0038	$n\pi^*_1$	110 (HOMO-7) → 118 (LUMO) (35%)
				$n\pi^*_2$	109 (HOMO-8) → 118 (LUMO) (23%)
				$n\pi^*_3$	108 (HOMO-9) → 118 (LUMO) (20%)
	S_3	4.21	0.1774	$\pi\pi^*_2$	116 (HOMO-1) → 118 (LUMO) (51%)
				$\pi\pi^*_1$	117 (HOMO) → 118 (LUMO) (26%)
	S_4	4.58	0.0956	$\pi\pi^*_3$	115 (HOMO-2) → 118 (LUMO) (65%)
kaempferol	S_1	3.61	0.5306	$\pi\pi^*_1$	74 (HOMO) → 75 (LUMO) (79%)
	S_2	4.29	0.1166	$\pi\pi^*_2$	73 (HOMO-1) → 75 (LUMO) (52%)
				$\pi\pi^*_1$	74 (HOMO) → 75 (LUMO) (12%)
	S_3	4.36	0.0000	$n\pi^*_1$	69 (HOMO-5) → 75 (LUMO) (86%)
	S_4	4.62	0.0477	$\pi\pi^*_3$	72 (HOMO-2) → 75 (LUMO) (28%)
				$\pi\pi^*_4$	71 (HOMO-3) → 75 (LUMO) (16%)

1.4. Femtosecond transient electronic absorption spectroscopy

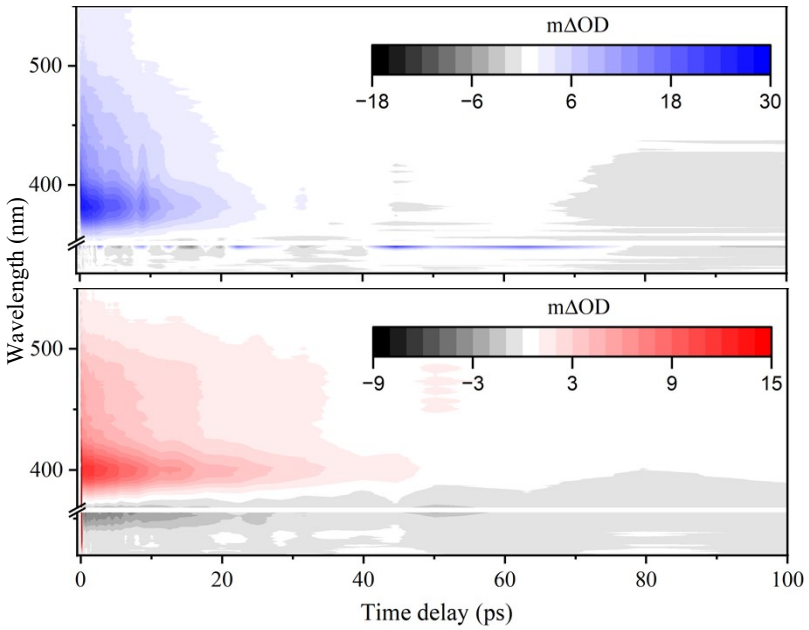

Figure S5. Collected transient absorption spectra of astragalin (top) and kaempferol (bottom) in 1,4-dioxane after photoexcitation with 347 nm and 364 nm light respectively.

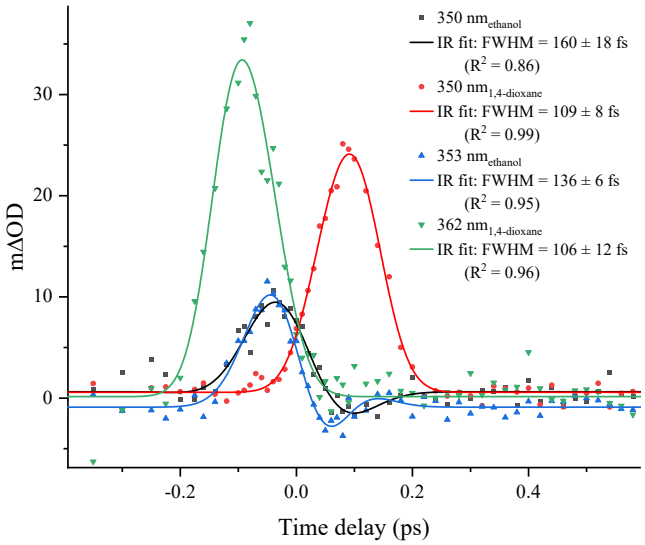

Determination of instrument response:

Figure S6. Kinetic TA profiles of solvent pumped at λ_{max} used in fs-TEAS experiments and probed at a wavelength near to this. Overlaid are fittings with a Gaussian function and its first and second derivatives, according to:

$$y = e^{-\left(\frac{t-t_0}{FWHM/2\sqrt{\ln 2}}\right)^2} \cdot (A + B(t-t_0) + C(t-t_0)^2)$$

where t_0 is time-zero and $FWHM$ is full width at half maximum of the convolution of two Gaussian pulses (i.e., 'pump' and 'probe'), to gauge instrument response function (IRF) for each experiment (see Table 2). Half of the respective IRF was reported as the error in each fs-TEAS

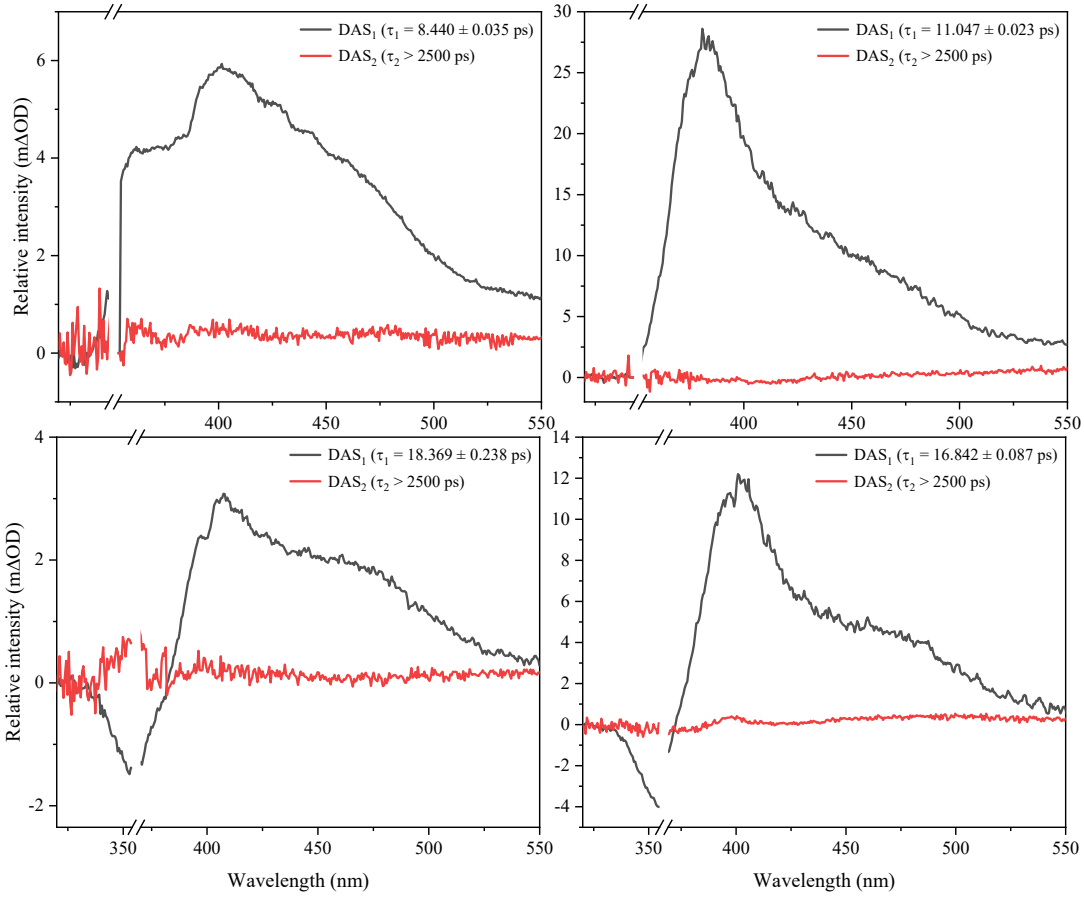

experiment, except in cases where the error extracted from global fitting was greater than this.

Figure S7. Decay associated spectra (DAS) corresponding to lifetimes extracted from global fitting of TA data for astragalin (top) and kaempferol (bottom) in ethanol (left) and 1,4-dioxane (right).

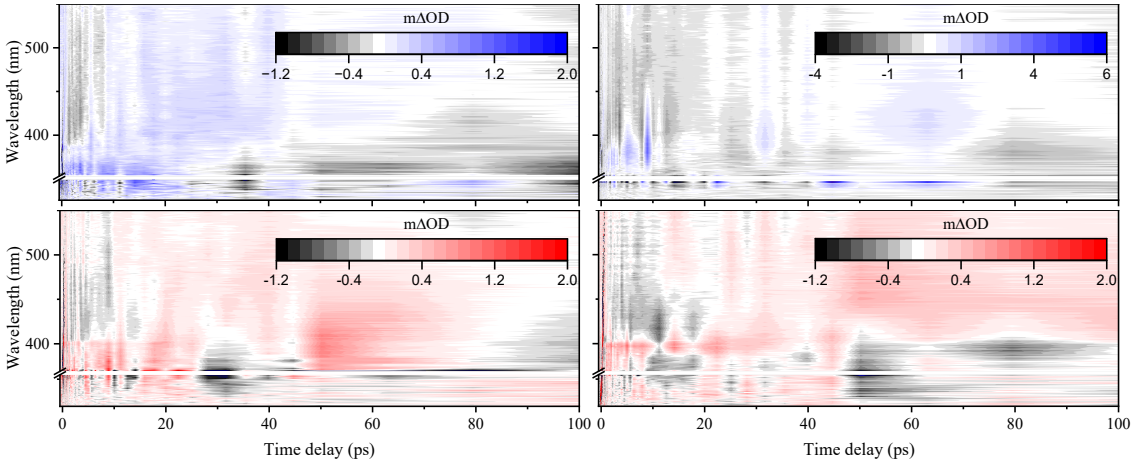

Figure S8. Residuals from global fitting of TA data for astragalin (top) and kaempferol (bottom) in ethanol (left) and 1,4-dioxane (right).

1.5. Photo-physics: nonadiabatic dynamics (NAD) simulations and conical intersections

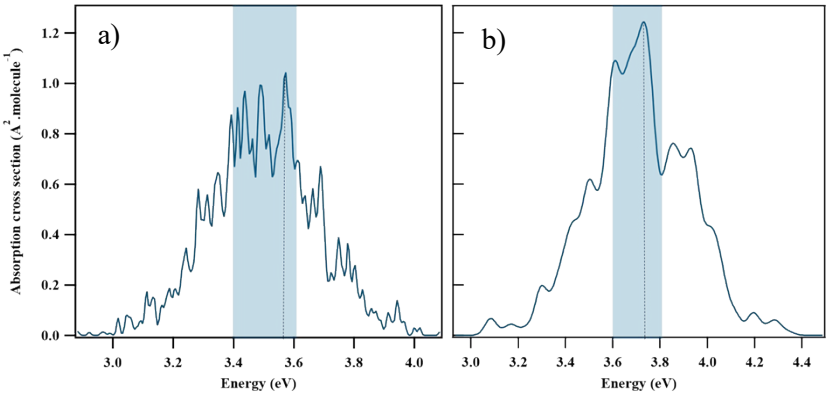

Figure S9. UV-visible absorption spectrum for (a) astragalin and (b) kaempferol, simulated using the TD-ωB97xD/cc-pVDZ method with 500 points, based on the $S_1 \leftarrow S_0$ electronic transition. The dashed line represents maximal absorption cross-section, and the shaded area indicates the spectral window from which initial conditions for dynamics trajectories were sampled.

Calculation of excited state lifetimes:

Excited state lifetimes and timescales for proton transfer have been obtained from NAD trajectories by fitting the fraction of excited state/initial proton tautomer population against time using the exponential decay function proposed by Mansour *et al.*[1]:

$$f(t) = f_{\infty} + Ae^{-x/\tau}, A = (1 - f_{\infty}),$$

where f_{∞} represents the fraction of population that does not decay within the given time frame and the excited state lifetime is t.

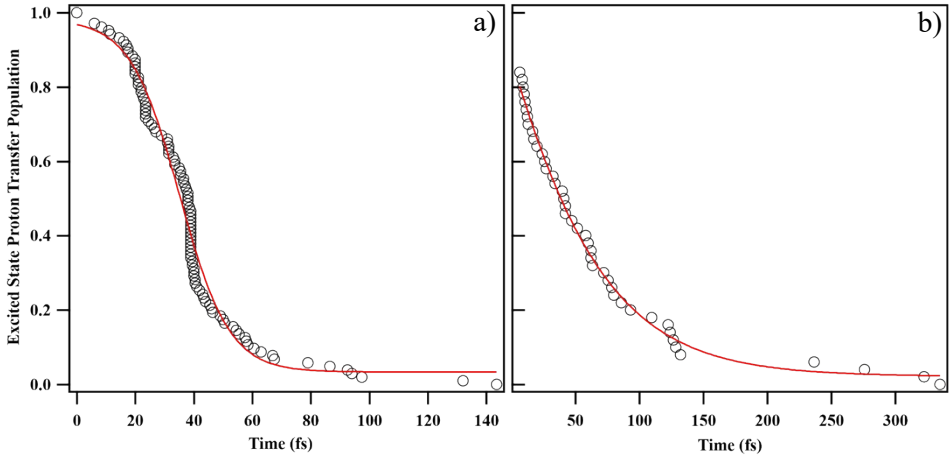

Figure S10. Proton transfer population in a) astragalin and b) kaempferol as a function of time, with fitted exponential decay function (red); extracted ESIPT lifetimes are 45 ± 5 fs and 75 ± 2 fs in astragalin and kaempferol, respectively.

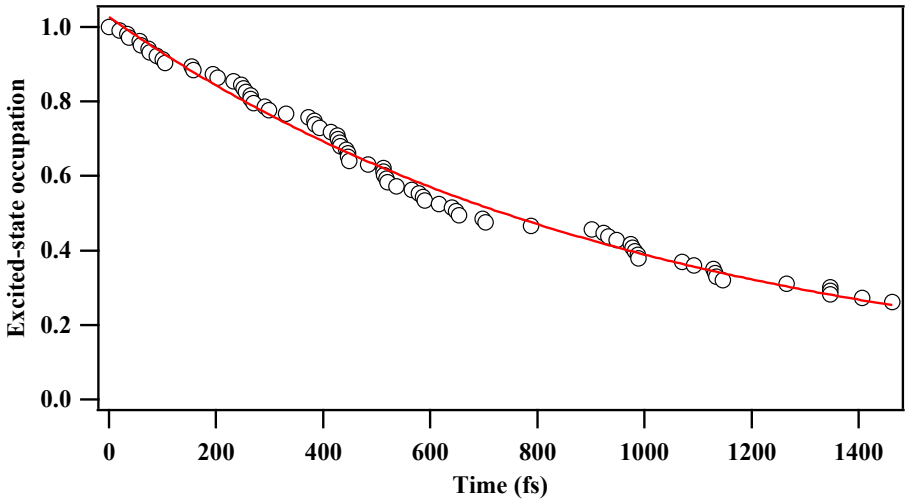

Figure S11. Excited state population in astragalin as a function of time, with fitted exponential decay function (red); extracted excited state lifetime is 984 ± 67 fs.

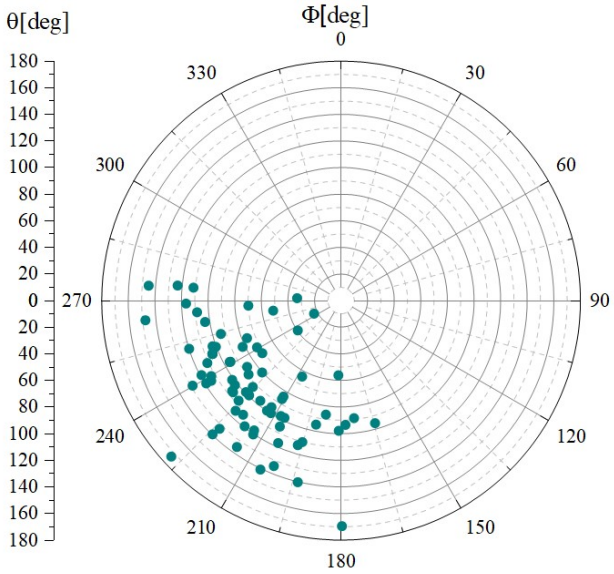

Figure S12. Polar plot showing distribution of Cremer−Pople parameters (θ, Φ) at S_1/S_0 crossing for ring C of astragalin.

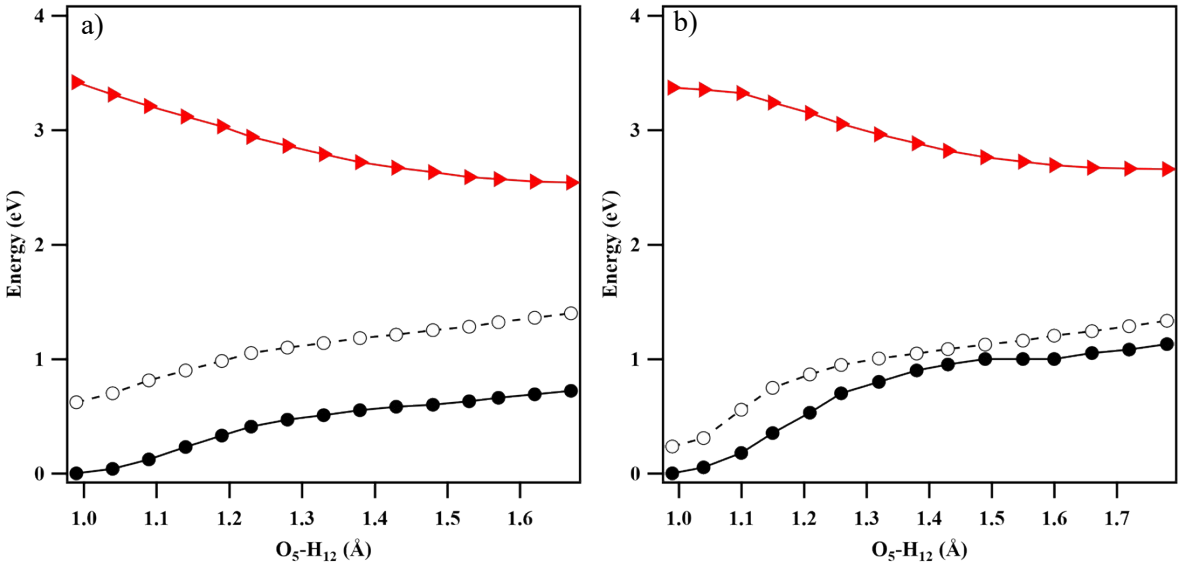

Figure S13. Relaxed reaction paths determined in S_0 (filled circles), energy profile of respective S_0 based on the optimized geometry in S_1 (empty circles), and S_1 energy profile (triangles) as a function of proton transfer coordinate for a) astragalin and b) kaempferol.

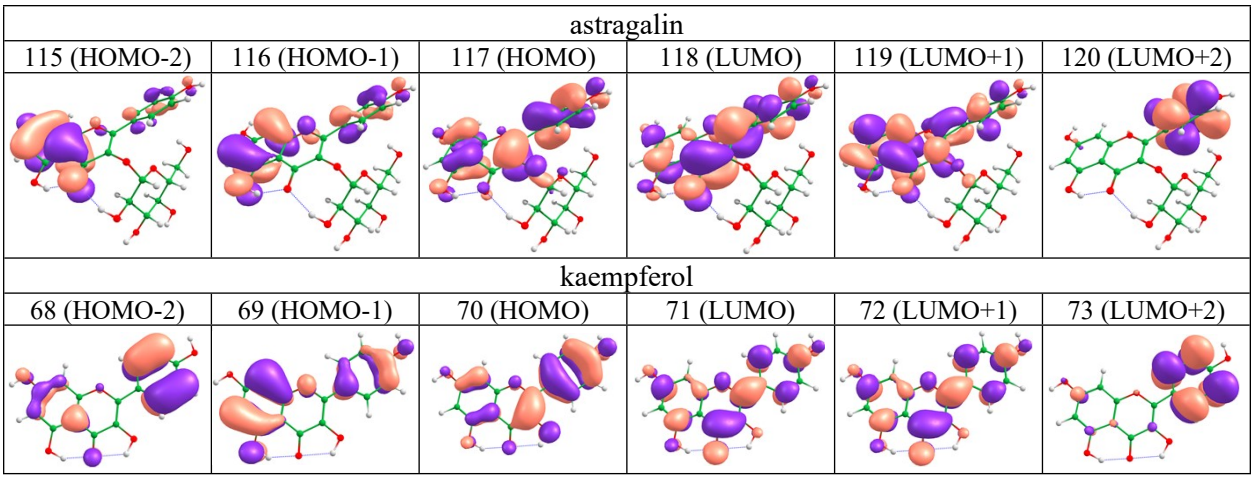

Figure S14. Selected valance MOs of astragalin and kaempferol conformers; three occupied and three virtual orbitals involved in CASSCF (6,6) geometry optimization of conical intersections.

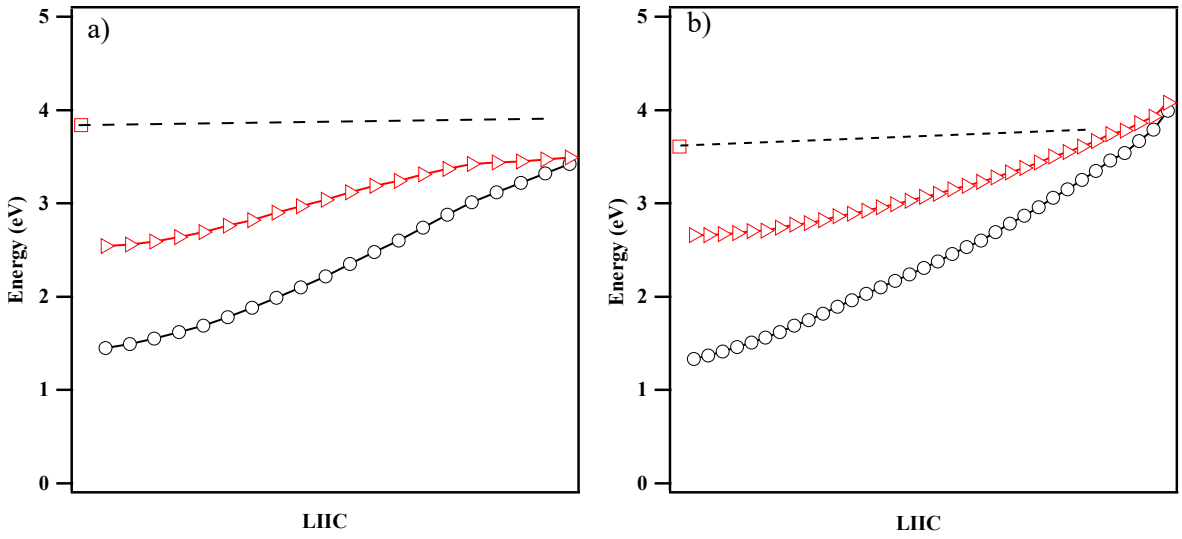

Figure S15. ADC(2) potential energy profiles, relative to the S_0 Franck-Condon geometry, of the electronic ground state (S_0, black circles) and the lowest $^1\pi\pi^*$ state (S_1, red triangles) along the LIIC coordinate. The LIIC connects the optimized S_1 and S_1/S_0 CI in each panel. The Franck-Condon vertical $S_1 \leftarrow S_0$ transition energy (S_1^{vert}, red square) is shown by a dashed line to facilitate comparison with CI energy.

Table S2. XYZ coordinates for the ground state optimized geometry of the astragalin at the MP2/cc-pVDZ level of theory.

52
C21H20O11

O	-3.082969689	-3.449589011	-3.095940779
O	-2.097913860	-1.460656667	-2.518181114
O	-2.649696127	-5.167620942	0.621540595
O	-3.261642612	-6.787363595	-1.634388930
O	-1.309125915	-2.751164356	0.029093746
O	-3.712352351	-4.858625944	-5.382102826
O	-5.426915519	-0.004062774	-2.924462691
O	-2.522158440	-0.289051567	-0.021064403
O	-4.046491884	1.116115234	1.571638736
O	-8.267120140	2.508807237	-0.022181269
O	-4.351555586	-2.656480895	-8.481640638
C	-2.326998696	-4.752972591	-0.696460767
C	-3.343066760	-5.372075708	-1.641140339
C	-2.326699797	-3.237286628	-0.819232926
C	-3.049596716	-4.887381441	-3.056770980
C	-2.088728326	-2.864976892	-2.281111978
C	-4.063585808	-5.333385378	-4.096607061
C	-3.283847315	-0.822712887	-2.218925364
C	-4.267328988	-0.673957126	-3.180197544
C	-3.416059987	-0.204128007	-0.906921115
C	-4.663772902	0.505260075	-0.681824168
C	-5.637669565	0.569671324	-1.697601399
C	-4.242254720	-1.189828236	-4.558059659
C	-4.942069730	1.145188037	0.569012744
C	-6.861480922	1.227196725	-1.523742686
C	-5.454255471	-1.589431301	-5.167481276
C	-3.044971651	-1.272600870	-5.300665864
C	-6.159383726	1.803563844	0.752741853
C	-7.108756537	1.842798377	-0.287850423
C	-5.467477005	-2.082801732	-6.475833427
C	-3.063542163	-1.753982972	-6.616884565
C	-4.271085119	-2.169852711	-7.212244125
H	-1.320030494	-5.124102631	-0.985691493
H	-4.354884602	-5.021558602	-1.345568663
H	-3.330898639	-2.868737233	-0.523153593
H	-2.043171661	-5.242583105	-3.362388051
H	-1.072159788	-3.176593505	-2.590317604
H	-5.065450716	-4.974723186	-3.780108656
H	-4.083103871	-6.432987314	-4.130894890
H	-2.050462557	-4.659304844	1.192063768
H	-3.257226816	-7.030237832	-0.694771142
H	-1.471631641	-1.787100559	0.075619441
H	-3.612562040	-3.900093774	-5.269164704
H	-7.581854752	1.252851902	-2.346741792
H	-6.389213464	-1.529019024	-4.603461681
H	-2.100745854	-0.964351804	-4.847207809
H	-6.376863892	2.291382543	1.705808739
H	-6.397189119	-2.416797455	-6.945516742
H	-2.126889194	-1.809720454	-7.184958199
H	-3.278866722	0.599992279	1.214061715
H	-8.824182013	2.460106507	-0.813339094
H	-3.449983021	-2.720324775	-8.830739064

Table S3. XYZ coordinates of the CASSCF (6,6)/6-31G* optimized geometry of the S_1/S_0 conical intersections of the astragalin.

O	-3.073031000	-3.710542000	-2.910689000
O	-2.182873000	-1.627412000	-2.478416000
O	-2.355039000	-5.250850000	0.793790000
O	-2.977357000	-6.986848000	-1.347039000
O	-1.179091000	-2.794920000	0.062858000
O	-3.921877000	-5.196322000	-5.097286000
O	-5.564754000	-0.228238000	-2.822786000
O	-2.572868000	-0.391272000	0.004746000
O	-4.035946000	1.603095000	1.215556000
O	-8.416463000	2.521934000	-0.225278000
O	-4.310603000	-1.887619000	-8.759802000
C	-2.122405000	-4.863893000	-0.557958000
C	-3.161567000	-5.577520000	-1.402246000
C	-2.219287000	-3.356875000	-0.716917000
C	-3.022116000	-5.158432000	-2.857122000
C	-2.071479000	-3.009623000	-2.189349000
C	-4.131921000	-5.642320000	-3.761581000
C	-3.324173000	-0.891547000	-2.205232000
C	-4.371870000	-0.846269000	-3.227386000
C	-3.450816000	-0.218619000	-1.049150000
C	-4.721482000	0.547746000	-0.780334000
C	-5.716999000	0.434835000	-1.689536000
C	-4.317911000	-1.125094000	-4.660129000
C	-4.902487000	1.385702000	0.353016000
C	-7.074016000	1.064701000	-1.584092000
C	-5.501479000	-1.205719000	-5.403200000
C	-3.109251000	-1.306684000	-5.331356000
C	-6.216812000	2.027794000	0.456392000
C	-7.291677000	1.832458000	-0.543238000
C	-5.479665000	-1.459416000	-6.760286000
C	-3.084664000	-1.567313000	-6.693960000
C	-4.268149000	-1.642108000	-7.407513000
H	-1.131910000	-5.186288000	-0.861542000
H	-4.147012000	-5.312867000	-1.035001000
H	-3.186572000	-3.022099000	-0.364051000
H	-2.067278000	-5.493898000	-3.244811000
H	-1.085894000	-3.268414000	-2.544736000
H	-5.084755000	-5.289926000	-3.383014000
H	-4.139641000	-6.718203000	-3.790532000
H	-1.774129000	-4.796125000	1.397072000
H	-2.951708000	-7.307353000	-0.450125000
H	-1.319336000	-1.856368000	0.191963000
H	-3.891588000	-4.245683000	-5.154278000
H	-7.770218000	0.868624000	-2.371057000
H	-6.442809000	-1.070887000	-4.912226000
H	-2.188165000	-1.249955000	-4.792026000
H	-6.396432000	2.689035000	1.278526000
H	-6.384756000	-1.525870000	-7.328664000
H	-2.141948000	-1.703073000	-7.190324000
H	-2.670092000	0.289153000	0.674463000
H	-9.144497000	2.439086000	-0.832020000
H	-3.470632000	-2.084998000	-9.156594000

Table S4. XYZ coordinates for the ground state optimized geometry of the kaempferol at the MP2/cc-pVDZ level of theory.

```
31
C15H10O6
```

C	0.252291723	-2.422351301	0.065694060
C	1.384282083	-3.258343547	-0.106477851
C	1.237793022	-4.646285465	-0.194703703
C	-0.034009938	-5.241023921	-0.114576962
C	-1.162861132	-4.419866613	0.056298833
C	-1.023208359	-3.029708947	0.145322890
H	2.380600746	-2.821283075	-0.171367388
H	2.111295830	-5.291693596	-0.327527208
O	-0.102716889	-6.602490274	-0.208615101
H	-2.162214500	-4.868026346	0.120809791
H	-1.912131229	-2.409653346	0.277838064
C	-2.263917933	1.514348059	0.602875653
C	-2.408848194	2.902773197	0.719943891
C	-0.972369644	0.998595155	0.438081379
C	0.161439594	1.837253222	0.389025539
C	-0.010286878	3.248264736	0.510216677
C	-1.294983223	3.769801419	0.674921140
C	1.468968134	1.253692118	0.218022734
H	-3.134433809	0.856485062	0.639441368
O	-3.678938366	3.373781833	0.879395304
O	1.051734763	4.075629256	0.467020570
H	-1.415547504	4.854365977	0.767196851
H	-3.625900201	4.338751165	0.945679389
O	-0.857144063	-0.356059521	0.326824731
C	0.368191213	-0.960593838	0.162270713
C	1.518509134	-0.194951204	0.106159316
O	2.764772325	-0.707880269	-0.053868804
O	2.549526372	1.904077189	0.160385975
H	-1.035856868	-6.852045578	-0.136039623
H	1.838261864	3.485306798	0.346084439
H	3.319701570	0.103110468	-0.048342083

Table S5. XYZ coordinates of the CASSCF (6,6)/6-31G* optimized geometry of the S_1/S_0 conical intersections resulting from out of plane deformation of kaempferol's B ring.

31
C15H10O6

C	0.260237000	-2.369212000	0.121033000
C	1.320931000	-3.191239000	-0.283086000
C	1.139992000	-4.549694000	-0.453111000
C	-0.101172000	-5.119879000	-0.223679000
C	-1.162669000	-4.328043000	0.176543000
C	-0.981169000	-2.964563000	0.345981000
H	2.285184000	-2.763854000	-0.452757000
H	1.949273000	-5.179465000	-0.761865000
O	-0.215022000	-6.479424000	-0.411812000
H	-2.128388000	-4.763131000	0.356779000
H	-1.810577000	-2.363548000	0.654730000
C	-2.300167000	1.502071000	0.823504000
C	-2.555515000	2.778032000	0.724084000
C	-0.869738000	1.070123000	0.588368000
C	0.171785000	1.890888000	0.341477000
C	-0.048534000	3.281137000	0.197718000
C	-1.445206000	3.707316000	0.367919000
C	1.528051000	1.248350000	0.198564000
H	-3.033507000	0.751935000	1.020232000
O	-3.818862000	3.294307000	0.828278000
O	0.829903000	4.117223000	-0.067294000
H	-1.658410000	4.739675000	0.169813000
H	-3.891588000	4.142944000	1.252548000
O	-0.748956000	-0.244933000	0.581028000
C	0.431253000	-0.933087000	0.293198000
C	1.617650000	-0.089749000	0.212651000
O	2.836097000	-0.723803000	0.265520000
O	2.666219000	1.996582000	0.463285000
H	-1.079287000	-6.833096000	-0.239630000
H	2.573610000	2.910153000	0.198112000
H	3.550584000	-0.100035000	0.369858000

Section 2: Preliminary Computational Study

Prior to our use of nonadiabatic dynamics simulations, a preliminary study of ethanolic kaempferol and astragalin was carried out. In this work an excited state intramolecular proton transfer (ESIPT) was identified, and evidence found that this transfer may be reversed in the ground state. What follows is an outline of the initial investigation.

General Settings

The computational workflow in our preliminary study used the ESTEEM Python package[2,3]. *Ab initio* calculations were performed using ORCA/5.0.2, a gaussian basis *ab initio* quantum chemistry package[4,5]. All ground and excited state properties were calculated using ORCA's implementations of DFT and linear-response TD-DFT respectively. The PBE0 hybrid exchange-correlation functional, def2-TZVP Karlsruhe basis set and D3BJ dispersion correction were used for all (TD-)DFT calculations[6–8]. A Conductor-like Polarizable Continuum Model (CPCM) was used to implicitly represent the solvent environment surrounding solute molecules[9]. For all implicit solvent calculations the CPCM model was parameterised with a dielectric constant (ϵ = 24.3) and refractive index (n = 1.361) to represent ethanol, in line with default vaules in ORCA. All geometry optimizations were carried out using the Broyden-Fletcher-Goldfarb-Shanno algorithm[10,11]. Unless otherwise specified, ORCA's default convergence thresholds were used for geometry optimizations.

2.1. Stable ground state geometries for astragalin

Ten coordinate files corresponding to plausible gas-phase conformers of astragalin (astragalin 1-10) were acquired from the PubChem database[12]. Ground state gas-phase geometry optimizations were performed, using these conformers as initial configurations. Ground state geometry optimizations of configurations resulting from the gas-phase relaxation were subsequently performed in implicit ethanol. The resulting configurations will hereafter be referrered to as GS-astragalin 1-10. The ground state total energies, Kohn-Sham (KS) HOMO-LUMO energy gaps, five lowest energy singlet-singlet vertical excitation energies (EE) and corresponding oscillator strengths were calculated for GS-astragalin 1-10. The transition densities for the five lowest energy singlet-singlet transitions and the HOMO & LUMO orbitals for GS-astragalin 8 were generated.

Table S6. Total energies in the ground state, Kohn Sham HOMO-LUMO gaps and electronic excitation energies ($S_1 \leftarrow S_0$) for GS-astragalin 1-10. Rows with emboldened text represent geometries with total energies >0.2 eVgreater than the lowest energy conformer.

System	S_0 Total Energy (eV)	KS HOMO-LUMO gap (eV)	EE (eV)
GS-astragalin 1	-44590.44036	4.4438	3.5648
GS-astragalin 2	-44590.34426	4.5157	3.6232
GS-astragalin 3	-44590.36072	4.3110	3.4565
GS-astragalin 4	**-44590.56723**	**4.3251**	**3.4555**
GS-astragalin 5	-44590.29548	4.5727	3.6628
GS-astragalin 6	**-44590.59520**	**4.3735**	**3.4886**
GS-astragalin 7	-44590.38761	4.4433	3.5648
GS-astragalin 8	**-44590.69437**	**4.3694**	**3.4856**
GS-astragalin 9	-44590.36801	4.4908	3.6052
GS-astragalin 10	-44590.12398	4.4662	3.5813

Table S7. The excitation energies and oscillator (Osc.) strengths corresponding to the 5 lowest-lying singlet-singlet transitions from the S_0 state for GS-astragalin 1-10.

System	EE $S_1 \leftarrow S_0$ (eV) /Osc. Strength	EE $S_2 \leftarrow S_0$ (eV) /Osc. Strength	EE $S_3 \leftarrow S_0$ (eV) /Osc. Strength	EE $S_4 \leftarrow S_0$ (eV) /Osc. Strength	EE $S_5 \leftarrow S_0$ (eV) /Osc. Strength
GS-astragalin 1	3.5648/0.5871	4.0399/0.3261	4.3095/0.0040	4.4375/0.1799	4.6928/0.1496
GS-astragalin 2	3.6232/0.5842	4.0851/0.2377	4.3811/0.0019	4.4792/0.1498	4.7595/0.0043
GS-astragalin 3	3.4565/0.6888	4.0150/0.2097	4.3170/0.0046	4.4375/0.1415	4.6716/0.0505
GS-astragalin 4	3.4555/0.7267	3.9223/0.2115	4.4154/0.1733	4.5250/0.0019	4.6471/0.0069
GS-astragalin 5	3.6628/0.4806	4.1163/0.2729	4.3080/0.0103	4.4808/0.1317	4.7650/0.1337
GS-astragalin 6	3.4886/0.6769	3.9360/0.1832	4.4013/0.1307	4.4841/0.0368	4.5835/0.0269
GS-astragalin	3.5648/0.6049	4.0691/0.2543	4.3687/0.0108	4.4615/0.1366	4.7089/0.0279

7					
GS-astragalin 8	3.4856/0.6523	3.9298/0.2110	4.3904/0.1422	4.4873/0.0239	4.6091/0.0488
GS-astragalin 9	3.6052/0.6516	4.0425/0.2599	4.3230/0.0005	4.4567/0.1537	4.7250/0.0036
GS-astragalin 10	3.5813/0.6480	4.0176/0.2122	4.3412/0.0063	4.4487/0.1430	4.5971/0.0254

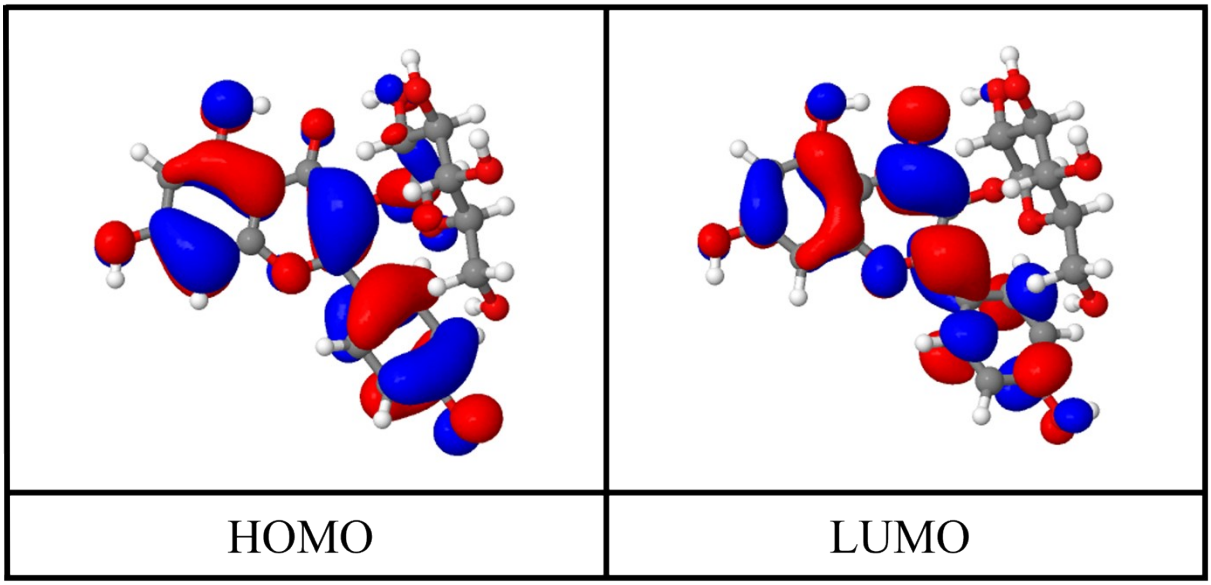

Figure S16. *HOMO and LUMO calculated for GS-astragalin 8.*

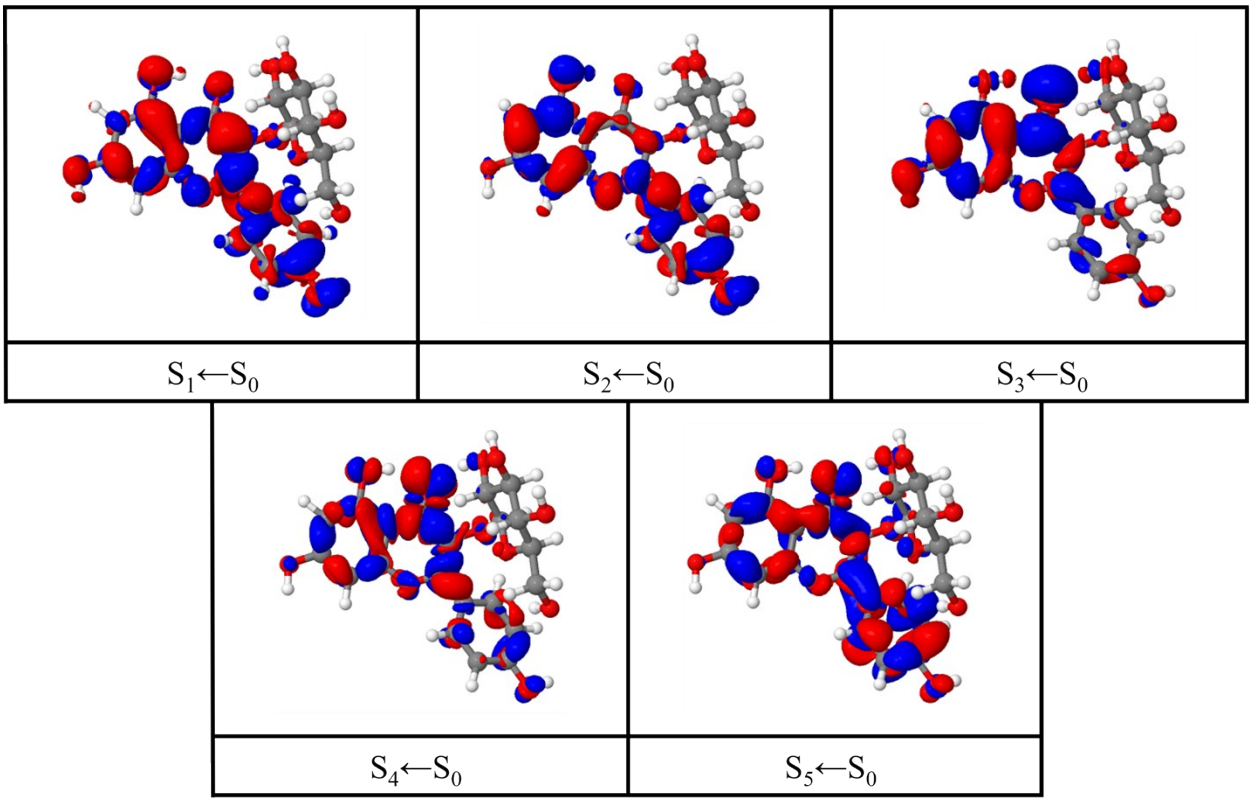

Figure S17. *Transition densities associated with transitions between S_0 and the five lowest energy excited singlet states, calculated for GS-astragalin 8.*

The total energies of the GS-astragalin conformers fall within 0.5704 eV of one another. From consideration of a Boltzmann distibution, geometries with total energies >0.2 eV above the lowest energy conformer (GS-astragalin 8) are unlikely to contribute significantly to the physical properties of the ensemble, so the following discussion of absorption results only pertains to GS-astragalin 4, 6 and 8. Predicted $S_1 \leftarrow S_0$ excitation energies corresponding to geometries optimized in the ground state (Table S7) fall within a range of 0.1172 eV, corresponding to absorptions at wavelengths from 355.4-358.8 nm. This shows good agreement with experimental data, where the peak maximum assigned to the $S_1 \leftarrow S_0$ transition was at 351 nm (3.5323 eV). For the three conformers, the $S_1 \leftarrow S_0$ transition has the highest predicted oscillator strength (Table S8), with an average of 0.6853 amongst conformers. It should be noted that oscillator strengths associated with the $S_2 \leftarrow S_0$ transition are also relatively significant, with an average of 0.2019. Our calculations predicted $S_2 \leftarrow S_0$ absorptions at wavelengths of 315-316.1 nm. In the experimental spectrum there was a relatively featureless peak at ~310 nm; our data suggests that this results from the $S_2 \leftarrow S_0$ transition, rather than from purely vibronic contributions associated with the

$S_1 \leftarrow S_0$ transition. The remaining three transitions ($S_3 \leftarrow S_0$, $S_4 \leftarrow S_0$ and $S_5 \leftarrow S_0$) correspond to absorption wavelengths/oscillator strengths of 280.8-282.4 nm/0.1487, 274.0-276.5 nm/0.0209 and 266.8-270.5 nm/0.0275, respectively. It is plausible that the experimental peak at 267 nm arises from a superposition of these transitions' contributions.

2.2. Excited state relaxation of astragalin

Geometries obtained in the initial ground state gas phase geometry relaxation (Section 1) were used as starting configurations for first excited singlet state gas phase geometry relaxations. The resulting configurations then underwent further relaxation in the first excited singlet state, solvated implicitly by ethanol. The resulting geometries will hereafter be referrered to as ES1-astragalin 1-10. Kohn Sham HOMO-LUMO gaps, $S_1 \leftarrow S_0$ vertical excitation energies and the corresponding oscillator strengths were then computed for ES1-astragalin 1-10.

Table S8. Total energies in the S_1 state, Kohn Sham HOMO-LUMO gaps, electronic excitation energies ($S_1 \leftarrow S_0$) and associated oscillator strengths for ES1-astragalin 1-10.

System	S_1 Total Energy (eV)	KS HOMO-LUMO gap (eV)	EE (eV) (5s.f.) /Osc. Strength
ES1-astragalin 1	-44587.68534	2.9422	2.0740/0.0997
ES1-astragalin 2	-44587.42467	3.0060	2.1274/0.1045
ES1-astragalin 3	-44587.53895	2.9876	2.1219/0.1254
ES1-astragalin 4	-44587.66068	2.9365	2.0599/0.0968
ES1-astragalin 5	-44587.38999	2.9813	2.1043/0.0951
ES1-astragalin 6	-44587.65550	2.9777	2.1032/0.0986
ES1-astragalin 7	-44587.53862	2.9352	2.0709/0.1010
ES1-astragalin 8	-44587.77266	2.9409	2.0705/0.0910
ES1-astragalin 9	-44587.49225	2.9843	2.1122/0.0930
ES1-astragalin 10	-44587.26768	2.9292	2.0565/0.0840

Contrary to the absorption data (Tables S7 & S8), determining which conformers provide physically relevant emission data is not simple. We cannot be certain which potential wells of the S_1 potential energy surface are most frequently occupied when excited state deactivation occurs, and cannot simply assume that the system relaxes to the lowest predicted energy. Relaxation to these lower energy geometries could potentially be hindered by excited state photochemistry and/or energy barriers. Hence, emission data from all conformers is discussed. The calculated energies of light emissions (Table S9) fall within a range of 0.0709 eV, with predicted emission

wavelengths ranging between ~582.8 nm and ~602.9 nm. Total energies of all conformers relaxed in the ground state fall within ~0.505 eV of one another. The average $S_1 \leftarrow S_0$ oscillator strength for the ES1-astragalin conformers was only ~16% of the average $S_1 \leftarrow S_0$ oscillator strength calculated for the GS-astragalin geometries (Table S8). This indicates a low propensity for emission, suggesting that nonradiative mechanisms of deactivation dominate astragalin's photochemistry.

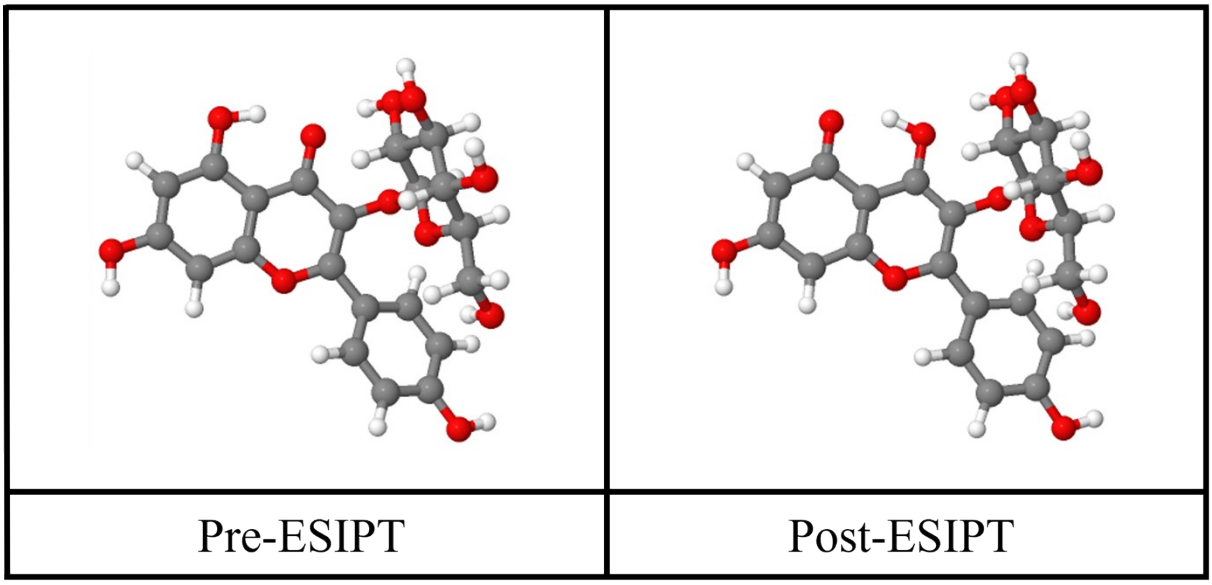

Figure S18. GS-astragalin 8 (left) and ES1-astragalin 8 (right) geometries.

In the excited state relaxation trajectories of all of the astragalin conformers, an ESIPT between the adjacent hydroxyl and carbonyl groups was observed (Fig. S17). We then optimised the ES1-astragalin geometries in the ground state to assess whether ground state intramolecular proton transfer (GSIPT), reversing the ESIPT, could plausibly lead to the regeneration of the GS astragalin geometries; a positive trend was observed for all conformers.

2.3. Search for stable ground and excited state geometries for kaempferol and astragalin

With the PubChem database suggesting only one plausible gas-phase conformer for kaempferol, we carried out a systematic search for stable geometries in the ground and first excited singlet state. We generated starting configurations with different orientations of two hydroxyl protons on the napthalene moiety, both of which appeared to be potential candidates for ESIPT. These

different orientations were generated for three tautomers that can be plausibly formed through ESIPT, hereafter referred to as enol, ketoO5 and ketoO3. To confirm the high stabilities of geometries identified in sections 1 & 2, we conducted a similar investigation for astragalin: we generated initial configurations with different orientations of the proton involved in ESIPT, for both the GS- (pre-ESIPT) and ES1-astragalin 8 (post-ESIPT) geometries (Fig. S19).

	Open	Closed
Pre-ESIPT	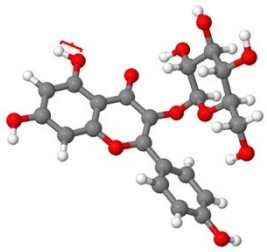	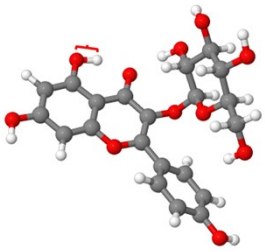
Post-ESIPT	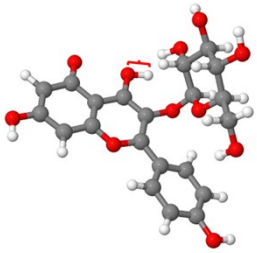	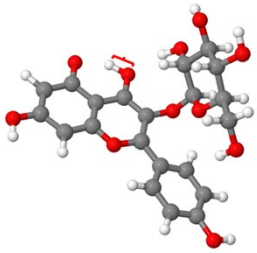

Figure S19. Starting geometries used in systematic search for stable conformers of astragalin.

	Open	Left	Right	Closed
Enol	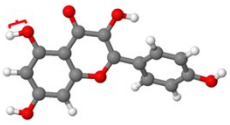	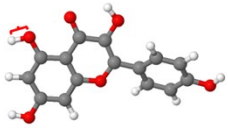	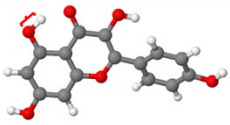	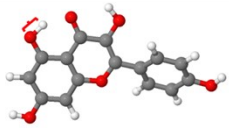
KetoO3	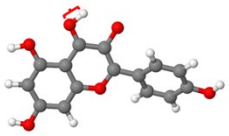	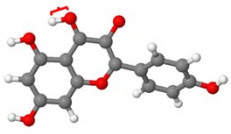	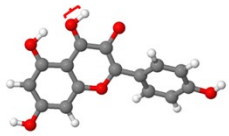	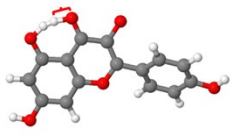
KetoO5	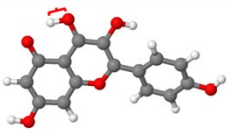	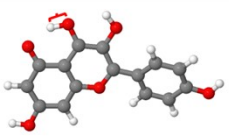	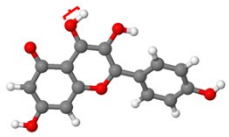	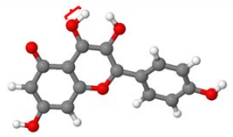

Figure S20. Starting geometries used in systematic search for stable conformers of kaempferol.

The initial configurations shown in Figures S18 and S19 were created by rotating and transplanting hydrogen atoms in GS-astragalin 8, ES1-astragalin 8 and a geometry of kaempferol obtained through the optimization of the PubChem suggested conformer of kaempferol in implicit ethanol. We then carried out relaxed scans of each of the initial configurations in implicit ethanol: the bonds marked with '}' in Figures S18 and S19 were constrained at a range of bond lengths, at 0.01 intervals, from 0.92-1.05 Å, and the remainder of the systems were relaxed using ORCA's TightOpt criteria. If an energy minimum was identified along this discrete series of fixed bond lengths, the corresponding geometry was then relaxed in implicit solvent with no constraints and the resulting total energies noted. The intention behind this initial relaxed scan was to inhibit intramolecular proton transfer, potentially enabling the systems to identify stable geometries local to their initial structures. This procedure was carried out in both the S_0 and S_1 states.

Table S9. Astragalin's relaxed energies (eV) of different geometries for tautomers in the ground state. '-' indicates that no local minimum was identified.

	Open	Closed
Pre-ESIPT	-44590.33953	-44590.69438
Post-ESIPT	-44589.68138	-

Table S10. Astragalin's relaxed energies (eV) of different geometries for tautomers in the S_1 state. '-' indicates that no local minimum was identified.

	Open	Closed
Pre-ESIPT	-44586.99606	-
Post-ESIPT	-	-44587.77264

Table S11. Kaempferol's relaxed energies (eV) of different geometries for tautomers in the ground state. '-' indicates that no local minimum was identified.

	Open	Left	Right	Closed
Enol	-27980.88496	-27981.14725	-27981.28335	-27981.46756
KetoO3	-27980.74636	-27980.51246	-27980.83530	-
KetoO5	-	-	-27980.41957	-

Table S12. Kaempferol's relaxed energies (eV) of different geometries for tautomers in the S_1 state. '-' indicates that no local minimum was identified.

	Open	Left	Right	Closed
Enol	-27977.58851	-27978.00452	-	-27978.40164
KetoO3	-27978.37506	-27978.27849	-27978.50108	-
KetoO5	-27978.45837	-27978.58301	-27978.20451	-

The most stable identified conformers of astragalin are 'Closed Pre-ESIPT' and 'Closed Post-ESIPT' in the ground and first excited singlet states, respectively (Tables S10 & S11). These geometries are visually indistinguishable from the GS-astragalin 8 and ES1-astragalin 8 geometries identified in Sections 1 & 2. The total energies found for astragalin 8 in Sections 1 & 2 agree closely with the energies of the 'Closed Pre-ESIPT' and 'Closed Post-ESIPT' geometries. This confirms that the methods outlined in Sections 1 & 2 did successfully identify the most stable conformers of astragalin in both the S_0 and S_1.

The most stable ground-state geometry of kaempferol is the 'Closed Enol' (Table S12). This geometry will hereafter be referred to as GS-CE kaempferol (Table S13). The most stable S_1 geometry of kaempferol is the 'Left KetoO5'. The five lowest energy singlet-singlet vertical excitation energies and oscillator strengths were then calculated for GS-CE kaempferol. The corresponding transition densities and the HOMO & LUMO orbitals were generated.

Table S13. Comparison of GS-astraglin 8 and GS-CE kaempferol's (kaempf CE) five lowest energy singlet-singlet excitations from their FC geometries. Excitation energies, oscillator strengths and orbitals most significantly involved (Orb. Inv.) for each transition are presented. 'Mixed' indicates that no set of orbitals has >0.5 weighting.

Transition	GS-astr 8 EE (eV)	GS-astr8 Osc. Strength	GS-astr 8 Orb. Inv.	kaempf CE EE (eV)	kaempf CE Osc. Strength	kaempf CE Orb. Inv.
$S_1 \leftarrow S_0$	3.4856	0.6523	HOMO→LUMO	3.2966	0.7948	HOMO→LUMO
$S_2 \leftarrow S_0$	3.9298	0.2110	HOMO-1→LUMO	3.9969	0.1831	HOMO-1→LUMO
$S_3 \leftarrow S_0$	4.3904	0.1422	HOMO-2→LUMO	4.4280	0.1033	HOMO-2→LUMO
$S_4 \leftarrow S_0$	4.4873	0.0239	Mixed	4.5616	0.0317	Mixed
$S_5 \leftarrow S_0$	4.6091	0.0488	HOMO→	4.6471	0.0008	HOMO-5→

			LUMO+1			LUMO

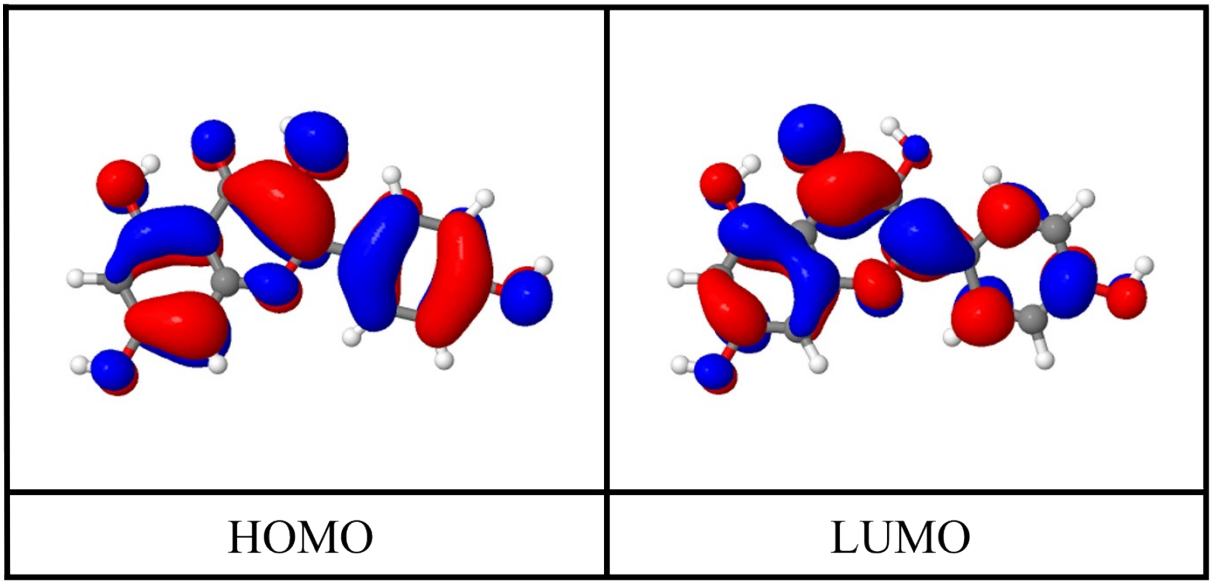

Figure S21. HOMO and LUMO calculated for GS-CE kaempferol.

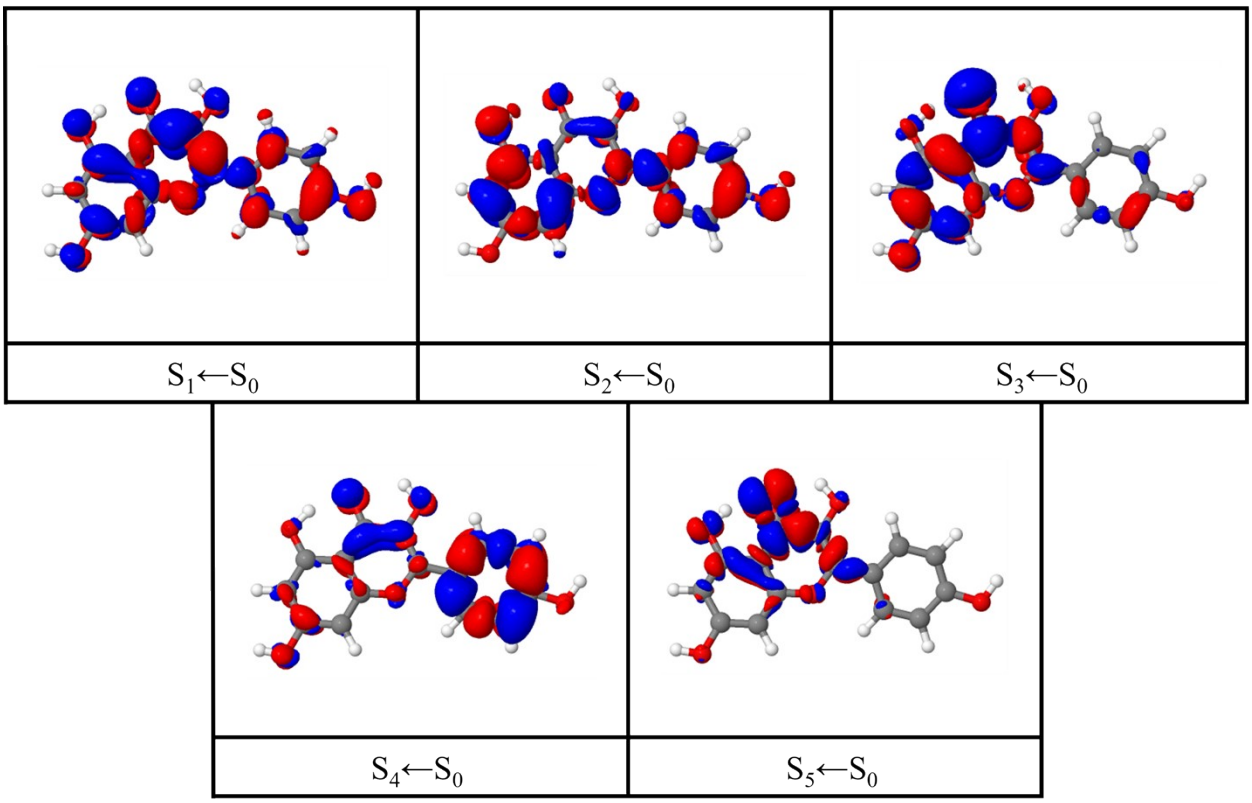

Figure S22. Transition densities associated with transitions between the ground singlet state and the five lowest energy excited singlet states, calculated for GS-CE kaempferol.

Our calculations predicted that ethanolic kaempferol would absorb at a wavelength of ~376.1 nm (Table S14), which shows good agreement with the experimental peak at 366 nm. Absorption is also predicted at ~310.2 nm, with a non-negligible oscillator strength of 0.1831. This falls within the range of the experimental peak from ~280-315 nm, suggesting that this corresponds to the $S_2 \leftarrow S_0$ transition, rather than being purely vibronic in nature. The remaining three transitions are relatively weak and plausibly contribute to the broad absorption at ~260-280 nm.

2.4. Excited state relaxation of astragalin

We optimised the GS-CE kaempferol geometry in implicit ethanol in the S_1 state; the resulting geometry will hereafter be referred to as ES1-CE kaempferol. We computed the $S_1 \leftarrow S_0$ vertical excitation energy (2.1340 eV) and corresponding oscillator strength (0.2136) for ES1-CE kaempferol. This oscillator strength is much lower than that of the GS-CE kaempferol geometry (0.7948), which indicates a low propensity for emission. This suggets that nonradiative mechanisms of relaxation play a significant role in this system.

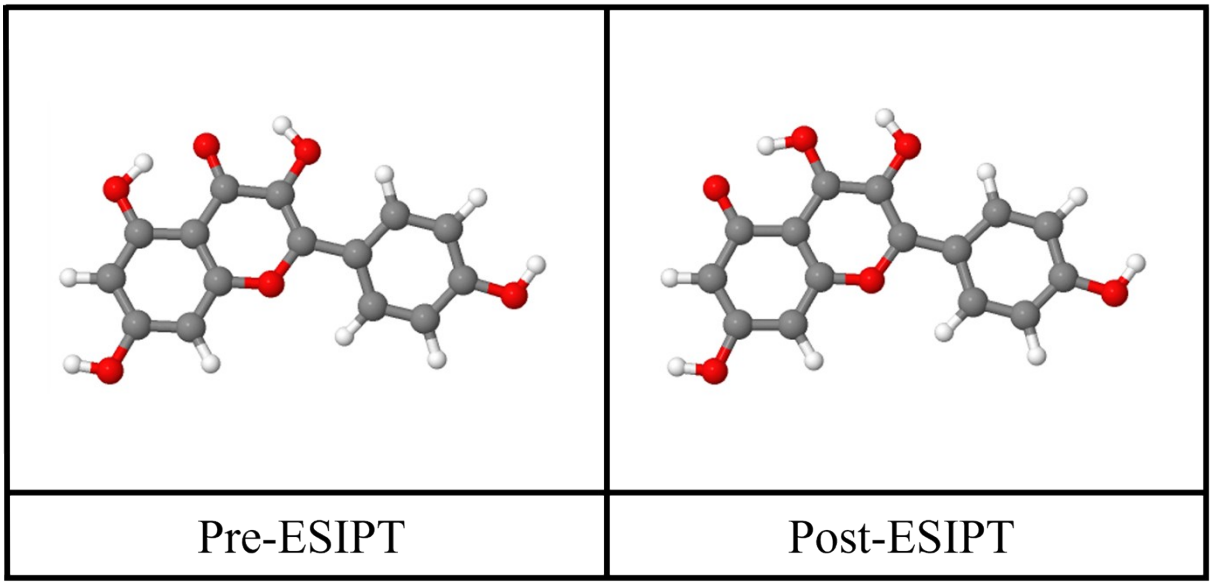

Figure S23. GS-CE kaempferol (left) and ES1-CE kaempferol (right) geometries.

In the first excited state relaxation trajectory an ESIPT was observed, with the proton of a hydroxyl group migrating to a proximal carbonyl group (Fig. S23). We then optimized the ES1-CE kaempferol geometry in the ground state to investigate the plausibility of GSIPT playing a

role in the relaxation mechanism of excited kaempferol. We did observe this GSIPT, regenerating the GS-CE kaempferol geometry.

2.5. Triplet involvement

We investigated the plausibility of phosphorescence involved in the relaxation of ethanolic astragalin and kaempferol from their first excited singlet states. If present, intersystem crossing (ISC) would be expected to occur around equilibrium geometries in the first excited singlet state. TD-DFT was used to calculate the spin-forbidden vertical excitation energies from the ground singlet state to the three lowest energy triplet states for the ES1-CE kaempferol (Section 4) and ES1-astragalin 1-10 (Section 2) geometries, in implicit ethanol.

Table S14. The vertical excitation energies corresponding to the $S_1 \leftarrow S_0$, $T_1 \leftarrow S_0$, $T_2 \leftarrow S_0$ and $T_3 \leftarrow S_0$ spin-forbidden transitions for ES1-CE kaempferol and ES1-astragalin 1-10.

System	$S_1 \leftarrow S_0$ EE (eV)	$T_1 \leftarrow S_0$ EE (eV)	$T_2 \leftarrow S_0$ EE (eV)	$T_3 \leftarrow S_0$ EE (eV)
ES1-CE Kaempf	2.1340	1.5527	2.3944	3.3556
ES1-astragalin 1	2.0740	1.6516	2.4239	3.2440
ES1-astragalin 2	2.1274	1.6996	2.4454	3.2423
ES1-astragalin 3	2.1219	1.6752	2.3991	3.2809
ES1-astragalin 4	2.0599	1.6500	2.3761	3.2321
ES1-astragalin 5	2.1043	1.6912	2.4546	3.2246
ES1-astragalin 6	2.1032	1.7007	2.3806	3.2271
ES1-astragalin 7	2.0709	1.6344	2.3648	3.2482
ES1-astragalin 8	2.0705	1.6721	2.3670	3.2154
ES1-astragalin 9	2.1122	1.7151	2.4469	3.2313
ES1-astragalin 10	2.0565	1.6627	2.3670	3.2037

As shown in Table S15, T_2 is the triplet state closest in energy to ES1-CE kaempferol's equilibrium geometry in the S_1 state, with a 0.2604 eV energy gap. The closest triplet state to S_1 out of all the conformers of ES1-astragalin was T_2 in ES1-astragalin 3, with a 0.2772 eV energy gap. These significant singlet-triplet energy gaps suggest that ISC would be relatively infrequent in these systems, meaning phosphorescence is likely an insignificant photophyiscal route.

2.6. Rotation of phenol moiety in kaempferol

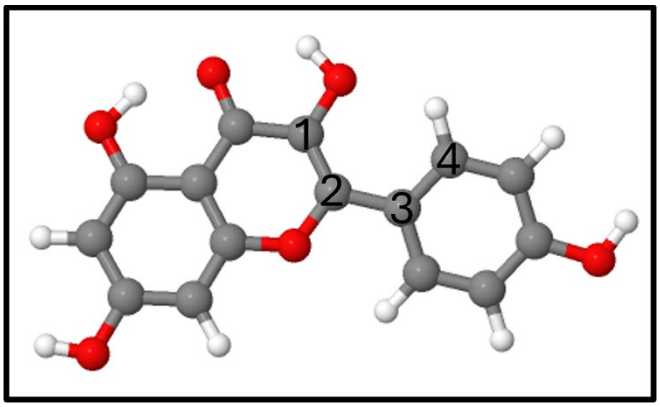

Figure S24. Kaempferol molecule with labels marking the four atoms that define the dihedral angle associated with the rotation of the phenol moiety in and out of the plane of the rest of the molecule.

With the phenol moiety (Fig. S23) in kaempferol having no obvious steric clashes preventing rotation in and out of the plane of the remainder of the molecule, it was important to assess the coupling of this rotation to the S_1 energy. If such a rotation resulted in a significantly higher S_1 energy, this motion could permit access to higher energy excited state pathways. We therefore carried out a relaxed scan in the ground state, using the GS-CE kaempferol geometry as a starting configuration and fixing the corresponding dihedral angle (involving atoms 1-4 in Fig. S18) at single degree intervals between ±20 °. This was done in implicit ethanol.

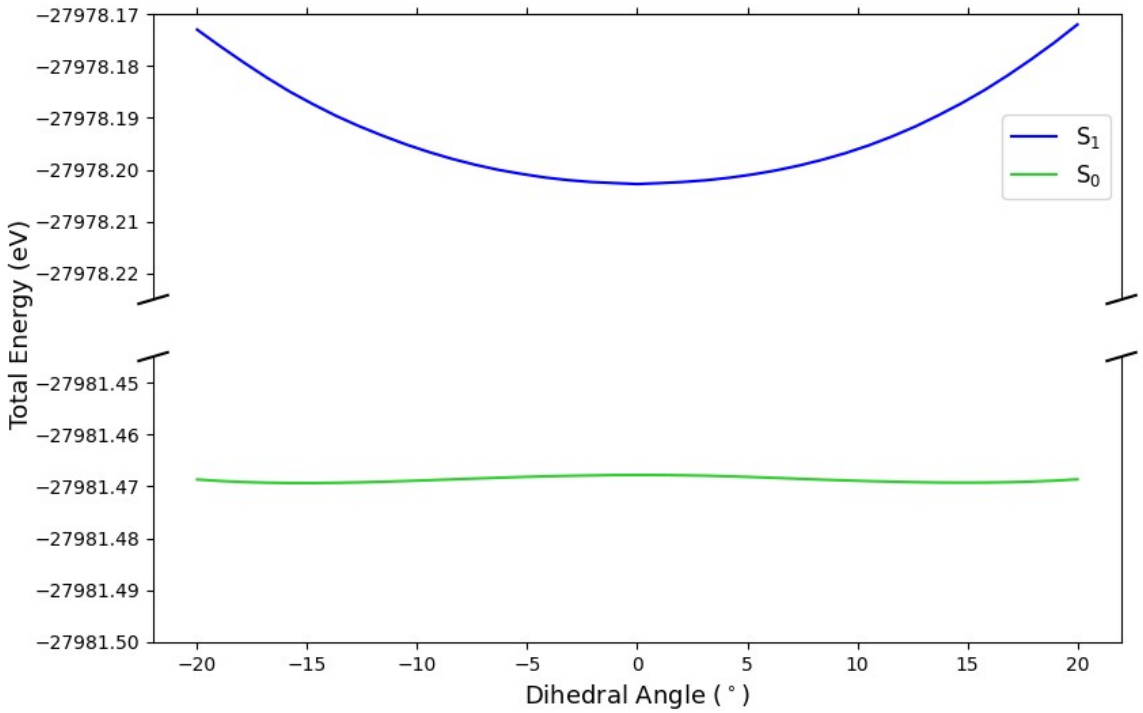

Figure S25. S_0 and S_1 energy surfaces corresponding to geometries obtained in the ground-state relaxed scan of GS-CE kaempferol geometry, with the dihedral angle defining the orientation of the phenol moiety relative to the rest of the molecule constrained between ±20°.

Whilst the total energy of the S_1 state is more strongly coupled to the rotation of the phenol group than to the total energy of S_0 state, the fluctuation in energy between ±20 ° is ~0.03 eV (Fig. S25). This small fluctuation is unlikely to result in a non-negligible proportion of systems accessing alternative excited state paths through phase space. Additionally, the weak coupling of the total energies of both states to the rotation of the phenol group suggests that this motion is unlikely to drive kaempferol towards an S_0/S_1 CI. This contrasts with deactivation pathways identified by Han et al.[13] for the closely related flavonoids luteolin and quercetin, where the rotation of a catechol substituent into the plane of the remainder of the molecules, following an initial ESIPT, leads the system to a CI.

References

(1) Mansour, R.; Toldo, J. M.; Mukherjee, S.; Pinheiro, M.; Barbatti, M. Temperature Effects on the Internal Conversion of Excited Adenine and Adenosine. *Phys. Chem. Chem. Phys.* **2023**, *25* (40), 27083–27093. https://doi.org/10.1039/D3CP03234E.

(2) Zuehlsdorff, T. J.; Haynes, P. D.; Payne, M. C.; Hine, N. D. M. Predicting Solvatochromic Shifts and Colours of a Solvated Organic Dye: The Example of Nile Red. *The Journal of Chemical Physics* **2017**, *146* (12), 124504. https://doi.org/10.1063/1.4979196.

(3) Turner, M. A. P.; Horbury, M. D.; Stavros, V. G.; Hine, N. D. M. Determination of Secondary Species in Solution through Pump-Selective Transient Absorption Spectroscopy and Explicit-Solvent TDDFT. *J. Phys. Chem. A* **2019**, *123* (4), 873–880. https://doi.org/10.1021/acs.jpca.8b11013.

(4) *The ORCA program system - Neese - 2012 - WIREs Computational Molecular Science - Wiley Online Library*. https://wires.onlinelibrary.wiley.com/doi/10.1002/wcms.81 (accessed 2025-04-23).

(5) Valeyev, E. Evaleev/Libint, 2025. https://github.com/evaleev/libint (accessed 2025-04-23).

(6) Adamo, C.; Barone, V. Toward Reliable Density Functional Methods without Adjustable Parameters: The PBE0 Model. *The Journal of Chemical Physics* **1999**, *110* (13), 6158–6170. https://doi.org/10.1063/1.478522.

(7) Grimme, S.; Ehrlich, S.; Goerigk, L. Effect of the Damping Function in Dispersion Corrected Density Functional Theory. *Journal of Computational Chemistry* **2011**, *32* (7), 1456–1465. https://doi.org/10.1002/jcc.21759.

(8) Hellweg, A.; Rappoport, D. Development of New Auxiliary Basis Functions of the Karlsruhe Segmented Contracted Basis Sets Including Diffuse Basis Functions (Def2-SVPD, Def2-TZVPPD, and Def2-QVPPD) for RI-MP2 and RI-CC Calculations. *Phys. Chem. Chem. Phys.* **2014**, *17* (2), 1010–1017. https://doi.org/10.1039/C4CP04286G.

(9) Barone, V.; Cossi, M. Quantum Calculation of Molecular Energies and Energy Gradients in Solution by a Conductor Solvent Model. *J. Phys. Chem. A* **1998**, *102* (11), 1995–2001. https://doi.org/10.1021/jp9716997.

(10) BROYDEN, C. G. The Convergence of a Class of Double-Rank Minimization Algorithms 1. General Considerations. *IMA Journal of Applied Mathematics* **1970**, *6* (1), 76–90. https://doi.org/10.1093/imamat/6.1.76.

(11) Fletcher, R. A New Approach to Variable Metric Algorithms. *The Computer Journal* **1970**, *13* (3), 317–322. https://doi.org/10.1093/comjnl/13.3.317.

(12) Bolton, E. E.; Wang, Y.; Thiessen, P. A.; Bryant, S. H. Chapter 12 - PubChem: Integrated Platform of Small Molecules and Biological Activities. In *Annual Reports in Computational Chemistry*; Wheeler, R. A., Spellmeyer, D. C., Eds.; Elsevier, 2008; Vol. 4, pp 217–241. https://doi.org/10.1016/S1574-1400(08)00012-1.

(13) Han, Y.; Jia, Y.; Wang, X.; Chen, Z.; Jin, P.; Jia, M.; Pan, H.; Sun, Z.; Chen, J. Ultrafast Excited State Dynamics of Two Non-Emissive Flavonoids That Undergo Excited State Intramolecular Proton Transfer in Solution. *Chemical Physics Letters* **2023**, *811*, 140189. https://doi.org/10.1016/j.cplett.2022.140189.